scientific reports

Check for updates

OPEN

Bioinformatic analysis reveals the relationship between macrophage infiltration and Cybb downregulation in hyperoxia-induced bronchopulmonary dysplasia

Yi He[1], Decai Li[1], Meiyu Zhang[2] & Fang Li[1]✉

Bronchopulmonary dysplasia (BPD) is the most common sequela of prematurity and is characterized by alveolar simplification and lung angiogenesis failure. The aim of this study was to explore the immune signatures of BPD. Differentially expressed gene analysis and immune infiltration analysis were conducted to identify key immune cell types and related genes by using the mRNA-seq dataset GSE25286. The expression patterns of key genes were validated in the scRNA-seq dataset GSE209664 and in experiments. The cell–cell crosstalk of key immune cells was explored with CellChat. We found that differentially expressed genes between BPD mice and controls were mostly enriched in leukocyte migration and M1 macrophages were highly enriched in BPD lungs. Hub genes (Cybb, Papss2, F7 and Fpr2) were validated at the single-cell level, among which the downregulation of Cybb was most closely related to macrophage infiltration. The reduced mRNA and protein levels of Cybb were further validated in animal experiments. Colocalization analysis of Cybb and macrophage markers demonstrated a significant decrease of Cybb in M1 macrophages. Cell–cell crosstalk found that alveolar epithelial cells interacted actively with macrophages through MIF-(CD74 + CD44) signalling. In conclusion, M1 macrophages played important roles in promoting BPD-like lung injury, which was correlated with a specific reduction of Cybb in macrophages and the potential activation of MIF signalling.

Keywords Bronchopulmonary dysplasia, Macrophage, Cybb, Immune infiltration, Cell–cell crosstalk

Abbreviations

BPD	Bronchopulmonary dysplasia
DEGs	Differentially expressed genes
WGCNA	Weighted gene co-expression network analysis
GEO	Gene expression omnibus
GO	Gene ontology
KEGG	Kyoto encyclopedia of genes and genomes
GS	Gene significance
MM	Module membership
STRING	Search tool for the retrieval of interacting genes

[1]Department of Pediatrics, Women and Children's Hospital of Chongqing Medical University, Chongqing Health Center for Women and Children; Chongqing Research Center for Prevention & Control of Maternal and Child Diseases and Public Health, Chongqing 401147, China. [2]Department of Neonatal Diagnosis and Treatment Center, Children's Hospital of Chongqing Medical University, National Clinical Research Center for Child Health and Disorders, Ministry of Education Key Laboratory of Child Development and Disorders, China International Science and Technology Cooperation Base of Child Development and Critical Disorders, Chongqing Key Laboratory of Pediatrics, Chongqing 400015, China. ✉email: rematalili@163.com

PPI	Protein–protein interaction
EPC	Edge percolated component
scRNA-seq	Single cell RNA sequence
qRT-PCR	Quantitative real-time polymerase chain reaction
UMAP	Uniform manifold approximation and projection
WT	Wild-type
AT1	Type I alveolar epithelial cells
AT2	Type II alveolar epithelial cells
MIF	Macrophage migration inhibitory factor
Klf4	Krüppel-like factor 4

Bronchopulmonary dysplasia (BPD), a multifactorial comorbidity of prematurity, that primarily characterized as lung impairment caused by hyperoxia and inflammation, is defined as the need for supplemental oxygen beyond 28 days postnatal or 36 weeks postmenstruation[1]. Perceptions on the pathophysiology of BPD have evolved from the time that it was first described as lung fibrosis and emphysema by Northway in 1967[2]; "new" BPD is mainly characterized by the underdevelopment of alveolarization and vascularization in the lungs, which affects more premature infants (especially those with a gestational age < 28 weeks)[3]. The sequelae of BPD can be long-lasting and profound, including susceptibility to respiratory infection, malnutrition and neurodevelopmental delay in childhood[4,5], as well as poor lung function and exercise capacity in adolescence and adulthood[6,7]. It is crucial to improve the management of BPD when considering the growing number of survival premature infants and the unreduced incidence of BPD.

An inflammatory cascade and increased inflammatory cytokines such as IL-6 and TNF-α have been observed in severe BPD patients and those who have died[8]. In addition to infectious conditions such as intrauterine inflammation or postnatal sepsis, sterile inflammation induced by hyperoxia may also be a driver of impaired lung development. Although hyperoxia is known to play important roles in BPD progression, clinical practice has suggested that reducing blood oxygen saturation is associated with increased mortality in preterm infants[9]. In addition to the direct effect of increased oxygen tension in the alveoli, the inflammatory response caused by lung injury under hyperoxia can also promote the progression of BPD. Given the necessity of life-saving oxygen therapy in critically ill preterm infants, managing the hyperoxia-induced inflammatory response may be an effective way to reduce lung injury in this high-risk population. Immune modulation is a promising strategy for treating BPD. Antibiotics such as macrolides have been reported to reduce the incidence of BPD in infants colonized by *Ureaplasma urealyticum*[10]. Anti-inflammatory therapies including steroids, pharmacological inhibitors of inflammation and cellular therapies have shown efficacy in improving BPD outcomes; however, pharmacological inhibitors are poorly developed due to a lack of effective immune targets[11]. Synthetic IL-1 antagonists, which are drugsfor neonatal multisystem inflammatory syndrome, have been reported to attenuate BPD-like lung pathology in mice and rats[12,13]; however, data on their clinical use in infants with BPD are still lacking. IL-6 and CXCL10 signalling are involved in the proinflammatory polarization of macrophages, disruption of alveolar homeostasis and fibrotic remodelling of the lung matrix, and could also be potential therapeutic targets[14,15]. The exploration of immune cell infiltration patterns and key immune modulators can facilitate targeted interventions focusing on inflammation, which is vital for improving the management of BPD.

Currently, the immune mechanisms of BPD have not been fully elucidated. With the development of various bioinformatic tools and sequencing technology, it has become possible to study molecular mechanisms at the single–cell level. To explore the key immune cells and molecules involved in the development of BPD-like lung inflammation under hyperoxia, we searched for Gene Expression Omnibus (GEO) datasets related to the mRNA sequencing data of lung tissues from hyperoxia-induced BPD mice. The literature research retrieved the mRNA dataset GSE25286[16] and the single-cell mRNA sequence (scRNA-seq) dataset GSE209664[17], which share similar oxygen interventions for constructing BPD mouse models. In this study, we first compared the mRNA sequencing data of BPD mice and controls, and found that differentially expressed genes (DEGs) were enriched in immune-related pathways. Afterwards, we conducted immune infiltration analysis and screened immune-related genes with weighted gene coexpression network analysis (WGCNA). Finally, the expression patterns of key genes were validated in single-cell RNA data and our BPD mouse models induced by hyperoxia. Cell–cell crosstalk analysis focusing on key immune cells was conducted with CellChat to explore important immune signalling pathways.

Methods

Data source

To search for eligible GEO datasets, terms such as "bronchopulmonary dysplasia", "lung dysplasia", "BPD" or "hyperoxia" were applied with the restriction of mouse species and lung tissue mRNA expression profiling by array. The BPD gene expression dataset GSE25286 and the scRNA-seq dataset GSE209664 were downloaded from the GEO database (https://www.ncbi.nlm.nih.gov/geo/).

DEG identification and enrichment analysis

After normalization of the data, the R software "limma" package was used to select DEGs with a |log(fold change)|> 1 and adjusted P value < 0.05 between the BPD and control groups. The nonlinear least squares method was applied with lmFit and adjustment of the variance was performed with the eBayes function. The "ggplot2" and "ggvolcano" packages were used to construct heatmaps and volcano plots for visualization of the results[18]. To better understand the biological attributes of the DEGs, enrichment analysis for the Gene Ontology (GO) and Kyoto Encyclopedia of Genes and Genomes (KEGG) pathways was conducted by using the "ggplot2", "clusterProfiler"

and "org.Mm.eg.db" packages[19]. The adjusted method was set as "Benjamini & Hochberg" and the organism was limited to "*Mus musculus*". The top 20 significant enrichment terms with $P < 0.05$ were shown.

Immune cell infiltration analysis and WGCNA

To investigate the immune infiltration signatures of BPD lungs, the proportions of 22 immune cell types were predicted in samples from the GSE25286 dataset by using the CIBERSORT algorithm in the "IOBR" package[20]. The number of permutations was set to 200. The immune cell fractions in each sample were shown with a bar plot Comparisons of immune cell proportions between the BPD and control groups were performed, and the results are shown in box plots. $P < 0.05$ was considered to indicate statistical significance.

To explore the correlation between gene expression and immunophenotypes, WGCNA[21] was employed to identify the module genes, which used the differentially infiltrated immune cells as trait data. First, hierarchical cluster analysis was conducted to filter the outliers of gene expression matrices. A soft power of $\beta = 8$ was selected to construct a scale-free network. The adjacency matrix was constructed and converted to a topological overlap matrix. Modules with high similarity were clustered and merged. The cluster dendrogram and gene module colour were drawn with dynamic hybrid cutting technology (minModuleSize = 10, mergeCutHeight = 0.4). Afterwards, the correlations between modules and differentially infiltrating immune cells were calculated, and the correlation coefficients and P values were shown in a heatmap. The genes of the modules that were significantly related to the immunophenotype (with the criteria of gene significance $|GS| > 0.8$ and module membership $|MM| > 0.8$) overlapped with DEGs to screen for immune-related DEGs. The overlapprocess was shown by using a Venn diagram.

Hub genes and single cell analysis

To identify the protein–protein interactions (PPIs) and central hub genes, the immune-related DEGs were analysed with the Search Tool for the Retrieval of Interacting Genes (STRING) database and then imported into Cytoscape v.3.7.1 to visualize the networks[22]. A topological analysis of the network was performed to identify the hub nodes. The top 15 hub genes with the highest scores were selected by using the edge percolated component (EPC) algorithm of the cytoHubba plugin[23].

To validate the hub genes at the single-cell level, the processed data "GSE209664_Sampath_finalobject-3.rds" were downloaded. The analysis and visualization of the scRNA-seq data GSE209664 with the "ggstatsplot", "Seurat" and "SCP" packages were performed in R 4.2.2. The "ggbetweenstats", "CellDimPlot", "FeatureDimPlot" and "DotPlot" functions were used to visualize the cell clusters of the scRNA-seq data[24]. After using "FetchData" function to obtain gene expression data of genes, the varied expression of hub genes between BPD and control groups were compared using "ggbetweenstats" and shown by violin plot. The cell source gene expression of hub genes were extracted and visualized by "DotPlot" function.

Cell–cell crosstalk analysis

To further explore the role of macrophages in the pathogenesis of BPD and lung development, we analysed the ligand-receptor interactions between macrophage clusters and the major cells composing the lung (alveolar epithelial cells and endothelial cells) by using the "CellChat" package in R 4.2.2. The "Secreted Signalling" interaction part of the CellChat database was selected for cell–cell communication analysis. The ligands or receptors that were overexpressed in each cell type were identified by using the "identifyOverExpressedInteractions" function. The upregulated expression levels were then projected into an interaction network to predict ligand-receptor pairs by using the "computeCommunProb" and "computeCommunProbPathway" functions[25]. The above mentioned cell–cell crosstalk analysis was performed on both merged and separate data of BPD and control groups.

Validation in animal models

Animal model and lung tissues. C57BL/6J mice aged at 6–8 weeks, which were provided by the Experimental Animal Center of Chongqing Medical University, were used in the animal study. Within 24 h of birth, 12 neonatal mice were randomly divided into a hyperoxia group (85% oxygen, N = 6) and a room-air group (21% oxygen, N = 6). The experimental mice were exposed to hyperoxia after birth to induce BPD-like lung injury. Nursing dams were exchanged between experimental and control groups every 24 h to avoid the effect of oxygen toxicity in the dams. At postnatal Day14, the mice were euthanized via injection of pentobarbital sodium to obtain lung tissues after transcardial perfusion with PBS to remove blood cells. All of the animal experimental procedures were performed according to the National Health and Medical Research Council guidelines under the approval of the Ethics Committee of Children's Hospital of Chongqing Medical University (IACUC Issue No: CHCMU-IACUC20221227001). The reporting of all the animal experiments in the manuscript followed the recommendations in the ARRIVE guidelines.

Quantitative real-time polymerase chain reaction (qRT-PCR). The mRNA expression levels of the hub genes were estimated by using qRT-PCR. Total RNA was extracted from lung tissues with TRIzol reagent (Biogroud, China). Reverse transcription into cDNA was performed with a Prime Script RT reagent kit (Accurate Biology, China). Each sample was tested in triplicate and β-actin was used as an internal control. The relative expression level was analysed by using the $2^{-(\Delta Ct)}$ method. Primers were produced by PREMIER Biosoft and purchased from Tiantai Biotech (China). The sequences of the utilized primers are listed in Additional file 1.

Western blotting. The protein levels of key genes were estimated. Total protein was extracted from lung tissues by using RIPA lysis buffer (Biogroud, China) containing protease and and phosphatase inhibitors. Proteins were separated via SDS—PAGE and transferred onto nitrocellulose membranes. The membranes were probed with primary antibodies against NOX2 (1:2000; Proteintech), GAPDH (1:1000; Cell Signalling Technology) and KLF4 (1:1000; Proteintech), and were incubated overnight at 4 °C. After the membranes were washed, they were

incubated with HRP-conjugated secondary antibodies (1:2000; Proteintech) for 1 h at room temperature. The chemiluminescence signal was detected by using an enhanced chemiluminescence (ECL) system (Bioground, China) and analysed with ImageJ software.

Immunofluorescence assay. To explore the relationship between the Cybb expression pattern and the macrophage markers CD86 and CD206, an in-situ immunofluorescence assay was performed. Lung sections were incubated with primary antibodies, including anti-NOX2 (Proteintech, 19013-1-AP, 1:3000), anti-CD86 (Cell Signalling Technology, #19589, 1:3000) and anti-CD206 (Cell Signalling Technology, 24595S, 1:3000), at 4 °C overnight. For each primary antibody, the sections were subsequently incubated with the appropriate HRP-conjugated secondary antibody (AiFang Biological, AFIHC003) for 50 min at room temperature. The sections were incubated with DAPI (AiFang Biological, AFYG006) for 10 min at room temperature for nuclear staining. Fluorescence was detected and photographed by using an upright fluorescence microscope (Nikon Eclipse C1, Japan) and a microscopy imaging system (Nikon DS-U3, Japan). Six nonoverlapping areas of each section were randomly selected at 40× magnification. Fluorescence was quantified as previously described by using pixel density measurements in ImageJ software[26]. GraphPad Prism was used for conducting statistical analysis.

Ethics approval and consent to participate

All animal work was conducted in accordance with the National Health and Medical Research Council guidelines under the approval of the Ethics Committee of Children's Hospital of Chongqing Medical University (IACUC Issue No: CHCMU-IACUC20221227001). The reporting of all animal experiments in the manuscript follows the recommendations in the ARRIVE guidelines.

Results

Data selection and DEG analysis

The selection and details of the mRNA datasets are described in Table 1. Newborn mice were exposed to hyperoxia from the first day after birth to induce BPD-like lung injury, and mice placed under room air served as controls. Due to the fact that the BPD mouse models in GSE25286 and GSE209664 were constructed under similar oxygen saturation conditions for more than 14 days, they were chosen as the subsequent exploration set and validation set, respectively. The GSE25286 contained lung tissues from 6 hyperoxia-induced BPD mice and 4 wild-type (WT) mice under room air. The GSE209664 contained lung tissues from 6 BPD mice and 6 WT mice under room air. When considering the possible incomparability in lung pathology due to different interventional methods, GSE193187 and GSE211356 were not selected as the validation sets. The flowchart of the study design and analytical procedure are shown in Fig. 1. According to the selection criteria, a total of 788 genes were found to be differentially expressed between BPD and control mice, including 456 upregulated genes and 332 downregulated genes. Volcano plots and heatmapss of the DEGs are shown in Fig. 2A,B. The enrichment analysis revealed the top 20 GO terms and KEGG pathways associated with the most DEGs with statistical significance (Fig. 2C). GO enrichment analysis demonstrated that the DEGs were mostly related to leukocyte migration, ameboidal-type cell migration, cell substrate adhesion, mitotic cell cycle phase transition and cell chemotaxis, thus suggesting the potential participation of the immune microenvironment and matrix remodelling in the pathogenesis of BPD. KEGG enrichment analysis indicated that the primary pathways involved in the pathogenesis of BPD included PI3K-Akt signalling pathways, MAPK signalling pathways, focal adhesion, regulation of actin cytoskeleton and lipid and atherosclerosis.

Characteristics of immune cell infiltration

We applied the CIBERSORT algorithm to analyse the immune cell composition based on the mRNA-seq data of GSE25286. The immune cell fractions of each sample were displayed as a bar plot (Fig. 2D). Monocytes and CD4 + memory resting T cells constituted the majority of immune cells in lung tissues. As shown in the box plot (Fig. 2E), compared to those in control mice, the infiltration of M1 macrophages and resting NK cells was significantly greater in BPD mice ($P < 0.05$). The conversion of M2 macrophages to M1 macrophages is associated with a proinflammatory state, and increased infiltration of M1 macrophages possibly contributes to lung inflammation and developmental abnormalities in BPD.

Afterwards, M1 macrophages and resting NK cells were used as the trait data for WGCNA to retrieve immune-related genes. A soft-threshold power of 8 was selected (Fig. 3A) and 6 modules were identified after

Datasets	Experiment type	Platform	Oxygen saturation in BPD/WT	Oxygen duration	Numbers of BPD/WT	Selection
GSE25286	Expression profiling by array	GPL1261	80%/21%	14 days	3/2	Exploring set
				29 days	3/2	
GSE209664	Expression profiling by high throughput sequencing	GPL19057	85%/21%	14 days	6/6	Validation set
GSE193187	Expression profiling by high throughput sequencing	GPL24247	65%/21%	5 days	4/4	Excluded
GSE211356	Expression profiling by high throughput sequencing	GPL19057	95%/21%	5 days	6/3	Excluded

Table 1. The selection and details of mRNA datasets in this study. *BPD* bronchopulmonary dysplasia, *WT* wild type.

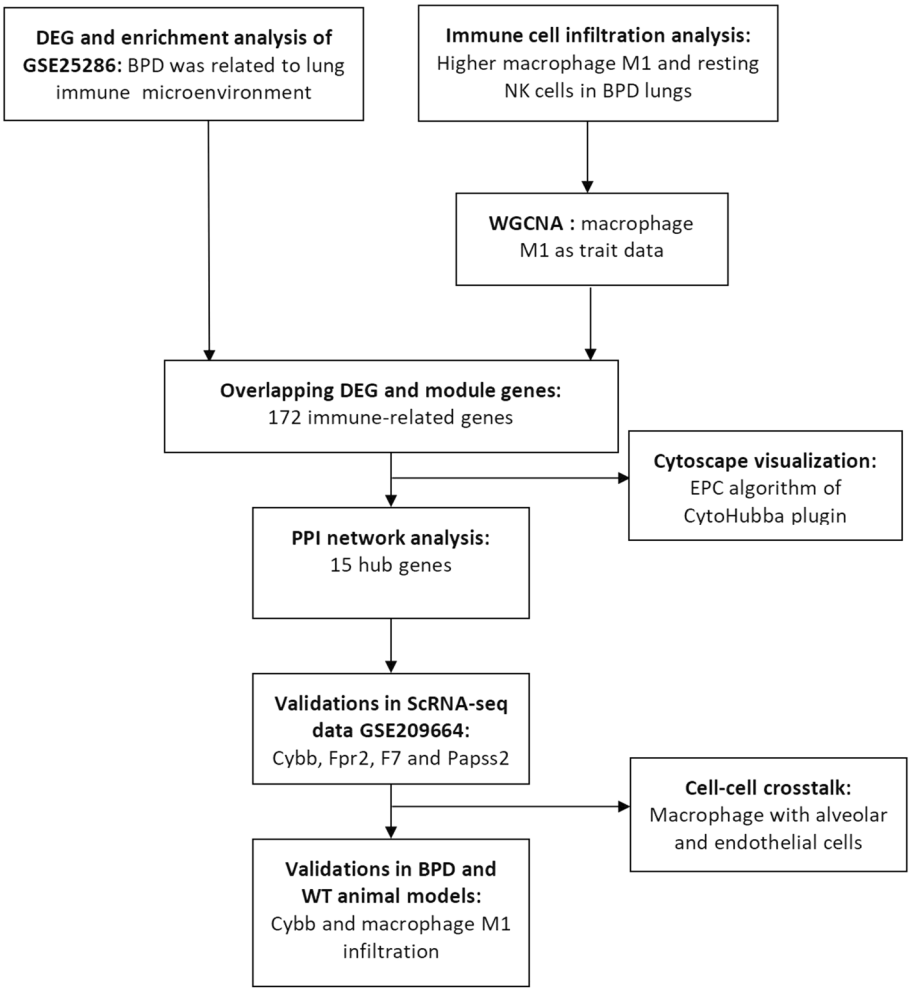

Fig. 1. Flow diagram of the study design.

clustering and merging similar module eigengenes (Fig. 3B). Correlation analysis (Fig. 3C) revealed that both BPD and differential immune cells were significantly related to the orange and yellow modules ($P < 0.05$). The correlation scatter plots between modules and traits are shown in Additional file 2. The genes in the orange and yellow modules subsequently intersected with the DEGs (Fig. 3D), thus yielding 172 immune-related genes (Additional file 3). When considering the important functions of macrophages compared to other immune cells in lung tissues, we focused on the relationships between these genes and macrophages in the subsequent analyses.

Hub gene identification and validation

In the PPI network of the 172 immune-related genes, topological analysis using the cytoHubba plugin and EPC algorithm revealed 15 hub genes, including Cybb, Pfn2, Papss2, Atp5a1, F7, Fpr2, Akt, CD79a, Dhfr, Clca1, Met, Sepw1, Mmp9, Ppbp and Fdps.) Cybb, Papss2, Pfn2, Atp5a1, F7, Fpr2 and Akt3 were relatively key nodes identified by EPC algorithm in the PPI network with deeper colour (Fig. 3E).First, we explored the cell source of the 15 hub genes in the scRNA-seq dataset GSE209664. Single-cell identification analysis was performed on the total 65,733 cells (38,223 cells from the BPD group and 27,510 cells from the control group). Cluster analysis, which were visualized by uniform manifold approximation and projection (UMAP), identified 25 types of cell clusters in the lung tissues and the number of cells in each cluster is shown in Additional file 4. Among the 65,733 single cells, 2492 were classified as alveolar macrophages, and 5447 were classified as other types of macrophages. We then examined the expression levels of the hub genes among the cell clusters. Among the 15 hub genes, 6 genes (Cybb, Mmp9, Fpr2, Cd79a, Papss2 and F7) were identified in the scRNA-seq dataset GSE209664. Cell source identification analysis revealed that Cybb, Fpr2 and F7 were expressed in large quantities in macrophages whether in BPD group (Fig. 4A) or control group (Fig. 4B). The expression pattern of the 3 hub genes in different cell types were visualized by using UMAP (Fig. 4C). Among the total single cells, 12,615 cells expressed Cybb (19.19%), which was the highest percentage among the 3 genes. Intuitively, Cybb and F7 were mainly expressed in macrophage clusters, and Fpr2 was mainly expressed in macrophage and neutrophils clusters. Since Cybb was the key node with highest EPC score in PPI network and had the closest relationship with macrophages, we mainly focused on the role of Cybb in subsequent analysis. We compared the expression of the hub genes

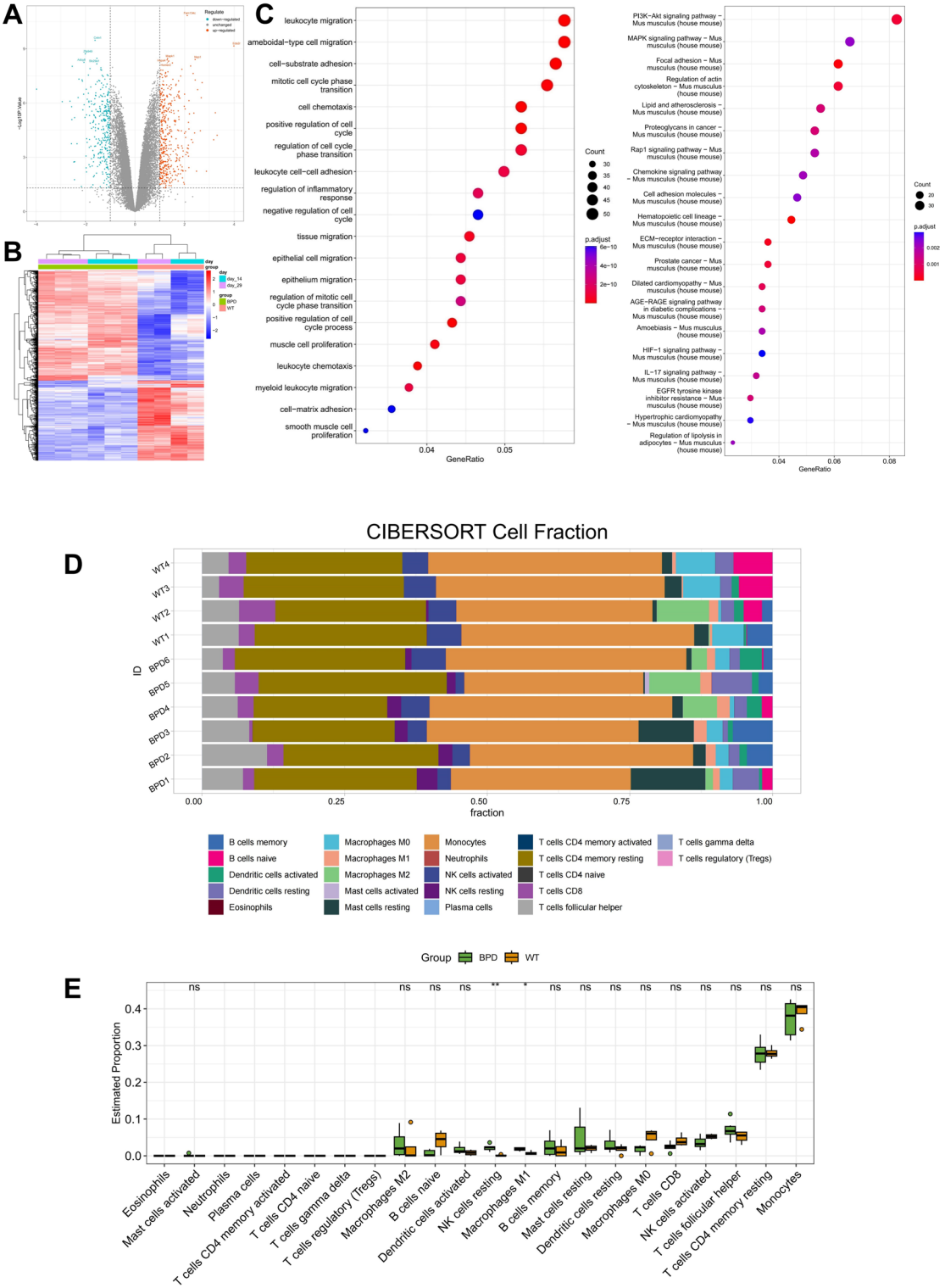

Fig. 2. Differentially expressed genes (DEGs), immune cell infiltration analysis and enrichment analysis in GSE25286. (**A**) The volcano plot of DEGs. Red dots represent up-regulated genes and blue dots represent down-regulated genes. (**B**) The heatmap of DEGs. The depth of the colour represents the expression level. The deeper the colour, the higher the expression level is. (**C**) The bubble plot of Gene Ontology (GO) enrichment analysis and Kyoto Encyclopedia of Genes and Genomes (KEGG) enrichment analysis. The dot size represents the count of DEGs involved and the colour represents the size of P values in the KEGG pathways. (**D**) The immune cell fractions in each sample of GSE25286. (**E**) The comparison of proportions of different immune cells between BPD and control groups.

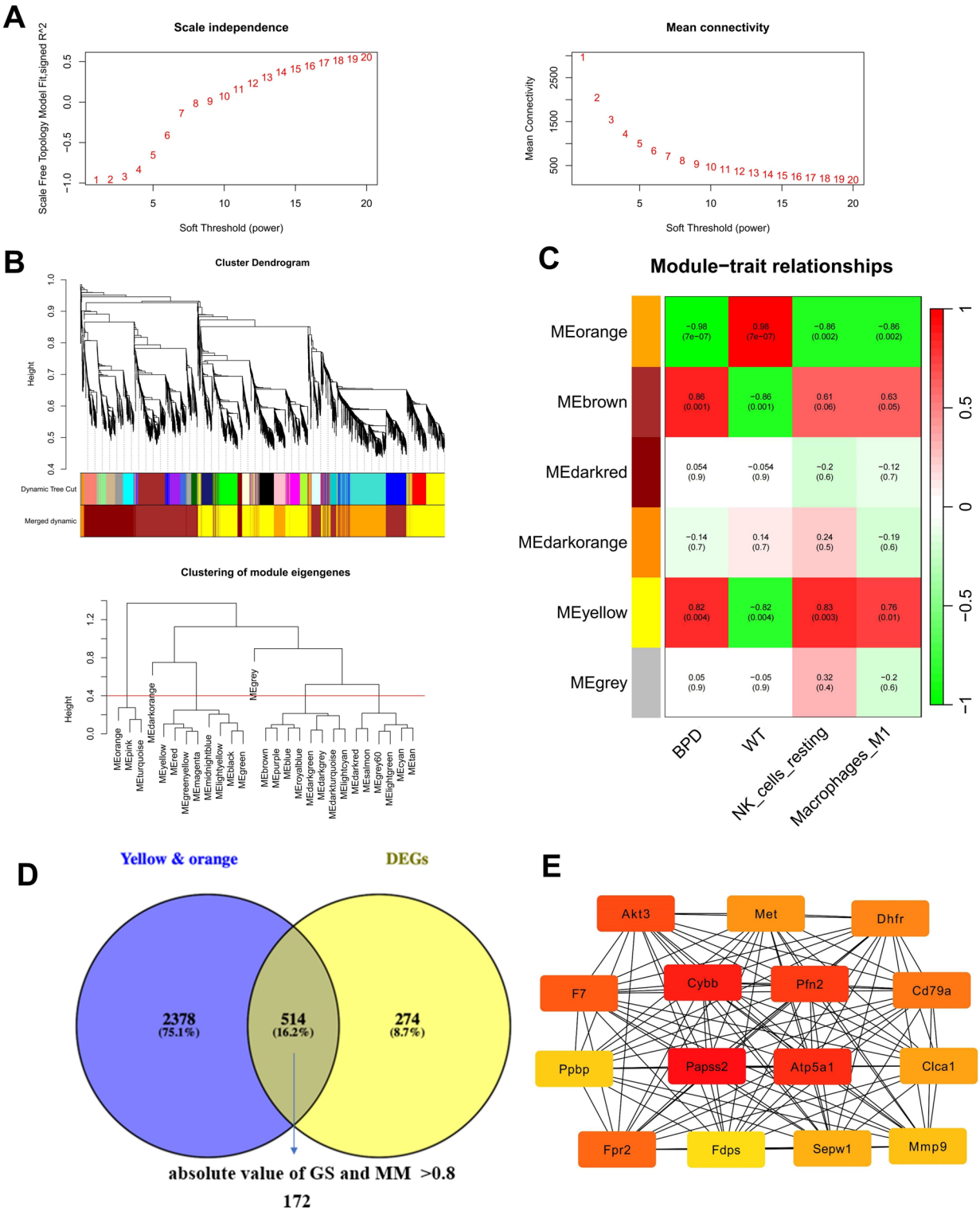

Fig. 3. WGCNA analysis using immune cells as trait data and hub gene selection. (**A**) Scale-free network analysis and mean connectivity analysis for various soft threshold powers. (**B**) The clustering dendrogram of differentially expressed genes (DEGs) constructed based on topological overlap matrix. (**C**) The heatmap of correlations between immune traits and modules. The coefficients and P values are shown in the box. (**D**) The Venn diagram showing the selection process of immune-related genes: intersection between module genes and DEGs. (**E**) Protein–protein interaction network of hub genes identified by imputing the immune-related genes to Cytoscape. The depth of red colour represented the scores of EPC algorithm.

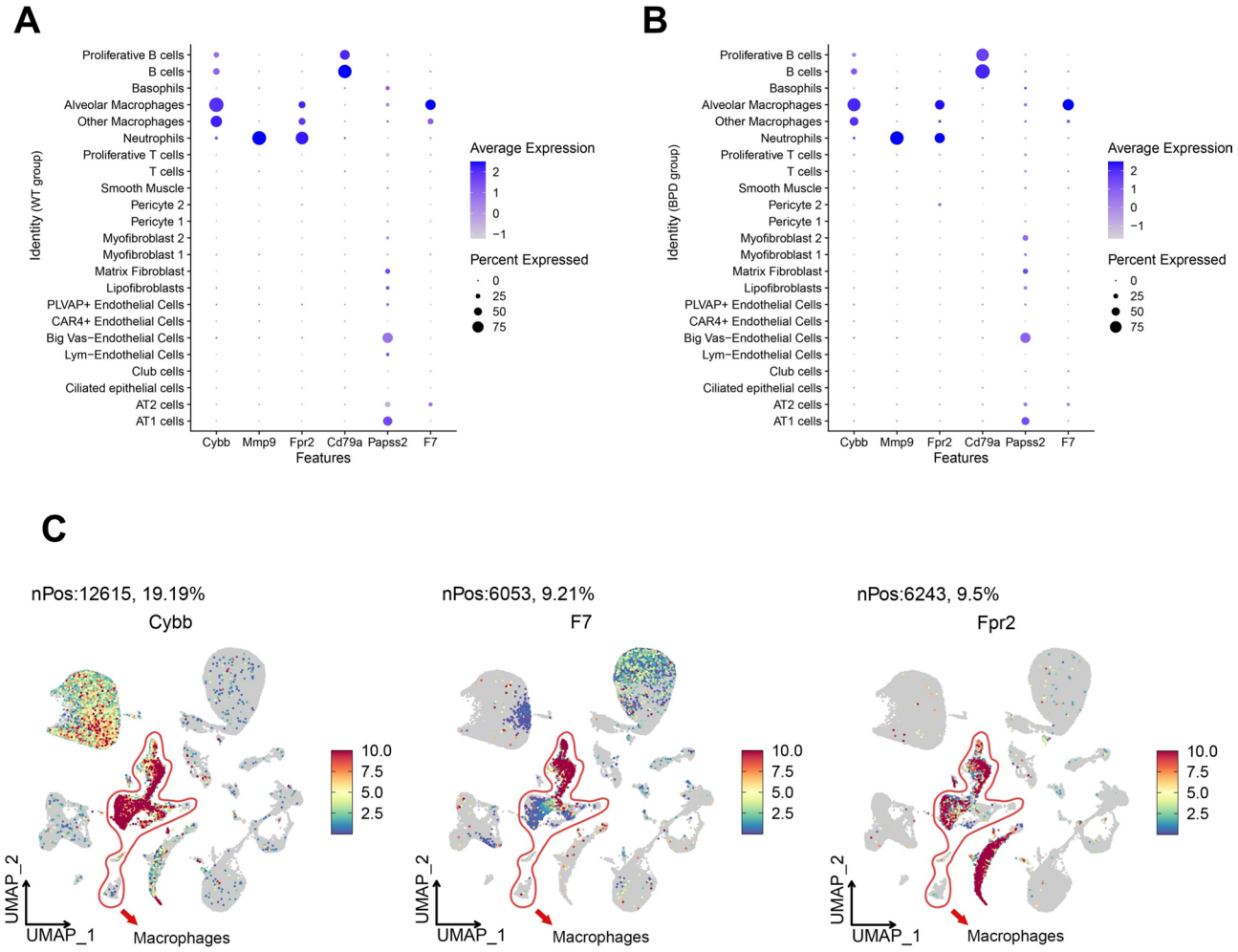

Fig. 4. Exploring the cell source of hub genes using scRNA-seq data GSE209664. (**A**) Dot plots of the expression pattern of the hub genes in different types of cells in WT group. (**B**) Dot plots of the expression pattern of the hub genes in different types of cells in BPD group. (**C**) The expression pattern of the 4 hub genes Cybb, F7 and Fpr2 in all single cells shown by UMAP algorithm. Cell clusters in red line represent macrophages. The range of colour represents the expression level of genes.

between the BPD and control groups by using the scRNA-seq data. Consistent with the prediction in the mRNA dataset GSE25286, the results in GSE209664 also indicated that Cybb was generally downregulated in the BPD group (Fig. 5A,B). Comparison of Cybb expression at the single-cell level between BPD and WT mice further demonstrated that the decrease was mainly due to the fact that the average expression and percentage of Cybb in macrophages were lower in BPD mice compared to WT (Fig. 5C) mice. These results suggested that Cybb expression predominantly decreased in macrophages under hyperoxia.

Cell–cell crosstalk among macrophages, alveolar epithelial cells and endothelial cells

The analysis was first conducted on the merged data of the BPD and control groups. Among the signal-sending cells, type I alveolar epithelial cells (AT1) had the most interactions with other cell types in tterms of quantity and strength; among the signal-receiving cells, CAR4 + endothelial cells were the most significant in terms of strength (Additional file 5A,B). In total, there were 11 ligand–receptor pairs among macrophages, alveolar epithelial cells and endothelial cells predicted by the "CellChat" package with statistical significance ($P < 0.01$) (Additional file 5C). The ligand–receptor signalling with the highest communication probability was macrophage migration inhibitory factor (MIF)-(CD74 + CD44) from type II alveolar epithelial cells (AT2) to macrophages, from AT2 to AT2, from AT1 to macrophages, and from AT1 to AT2, which suggested a close relationship between macrophages and alveolar epithelial cells. The incoming and outgoing signalling pathways in different cell clusters are shown in Additional file 5D. Macrophages mainly acted as signalling receivers involved in SEMA3, MIF, GALECTIN, CXCL, CCL and COMPLEMENT signalling pathways, whereas macrophages acted as signalling senders involved in GRN and CCL signalling pathways.

Afterwards, we explored cell–cell crosstalk in the BPD group and control group, respectively. As the signalling senders, macrophages only interacted with alveolar epithelial cells in WT controls, while interacted with alveolar epithelia cells and various endothelial cells in the BPD mice (Fig. 6A). AT1 and AT2 had more interaction

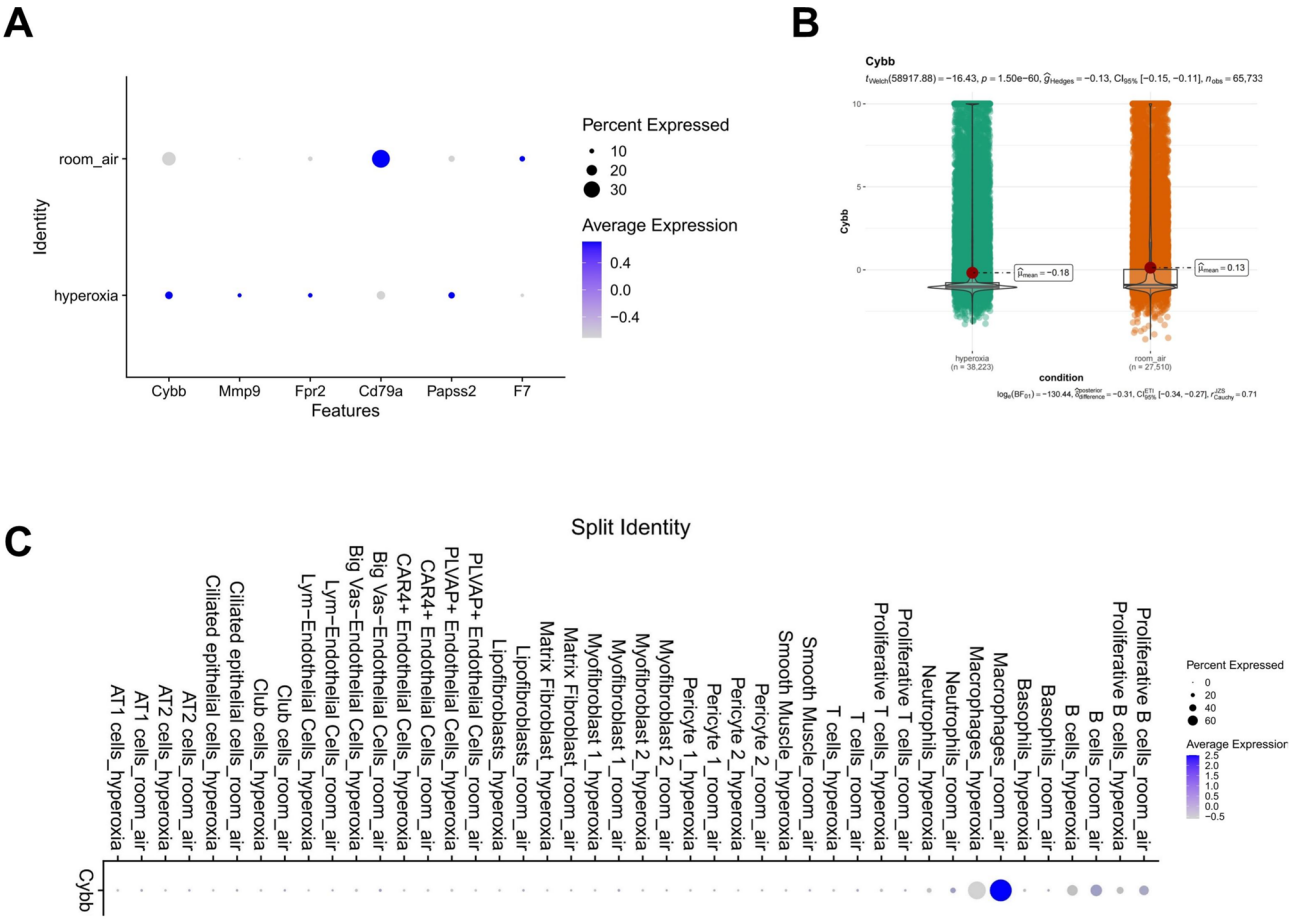

Fig. 5. Validating expression levels of hub genes in scRNA-seq data GSE209664 identified downregulation of Cybb inmacrophages of the BPD group. (**A**) Dot plots of the expression pattern of the hub genes in the WT and BPD group. The size of the circles indicates the percentages of cells expressing the gene in different cell types; the colour represents the average expression levels of the gene. (**B**) Comparison of the expression level of Cybb between BPD and WT groups. (**C**) The dot plot of the expression pattern of Cybb in the BPD and WT groups.

counts in the BPD group than in the WT group, whereas Lym-endothelial cells showed the opposite trend. The interaction strength of these cells remained unchanged in general, except for the observation that the interaction strength of AT2 was increased in the BPD group (Fig. 6B). In the BPD group, the ligand–receptor signalling pathways with the highest communication probability was still MIF-(CD74 + CD44) from AT2 to macrophages, from AT2 to AT2 and from AT1 to macrophages, the probability of which was not high in the WT group (Fig. 6C). In addition, the relative importance of each cell type in MIF signalling varied between BPD and WT mice, which indicated increased involvement of macrophages, especially as signalling receivers, in BPD mice. In contrast to the major interaction between AT2 and endothelial cells in WT mice, macrophages became the main receiver of MIF signalling in BPD mice (Fig. 6D). Collectively, these results suggested that macrophages were more active and interacted more with alveolar epithelial cells in BPD mice through MIF-(CD74 + CD44) signalling than in WT mice.

Validation of the hub genes and key pathways in mouse models

The differences in lung morphometry and body weight between the hyperoxia and room-air groups indicated that we successfully established BPD-like mouse models (Additional file 6). To further validate the roles of macrophages-related genes in BPD, the gene expression levels between the hyperoxia group (BPD) and room-air group (WT) were further compared in our mouse models. In accordance with the bioinformatic analysis, the validation experiments revealed that the mRNA expression levels of the 3 macrophage-related genes (Cybb, Fpr2 and F7) were downregulated in the BPD group (Fig. 7A). Due to the fact that M1 macrophages was significantly upregulated in BPD mice and that Cybb was the most closely related to macrophages in our previous analysis, we focused on macrophage infiltrations and Cybb expression. At the protein level, Krüppel-like factor 4 (Klf4), the reduction of which is known to indicate macrophages M1 polarization, was downregulated in the hyperoxia group. The level of the Cybb protein was lower in the hyperoxia group as expected (Fig. 7B). The full-length blots of Cybb and Klf4 are included in Additional file 7. We subsequently detected the relationships of Cybb expression patterns and macrophage infiltration via immunofluorescence. The number of M1 macrophages (marked with CD86) was evidently greater in BPD than in WT. Interestingly, we detected colocalization of Cybb and CD86 in

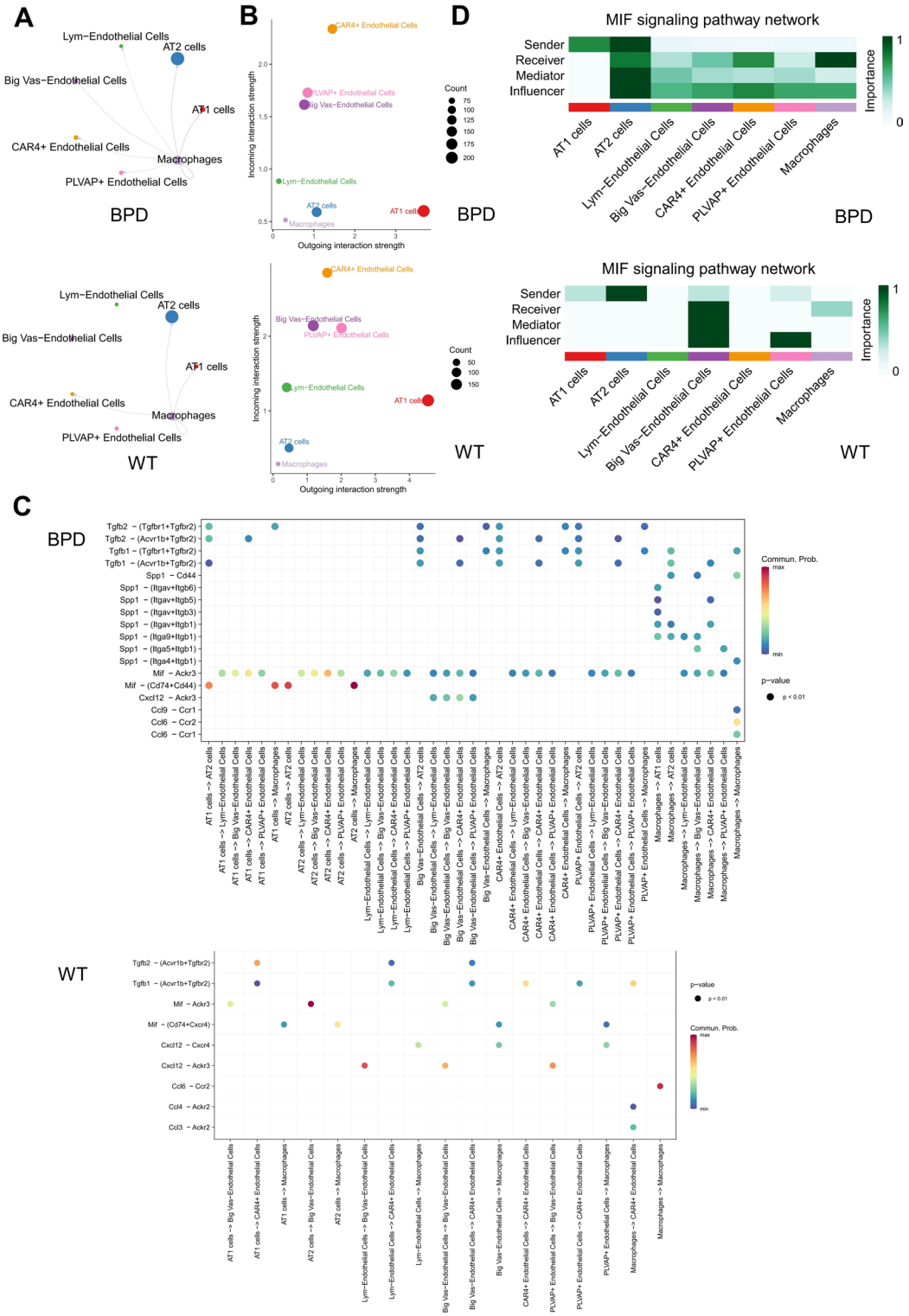

Fig. 6. Comparison of cell–cell crosstalk patterns between BPD and controls in the scRNA-seq data. (**A**) Signalling to alveolar cells and endothelial cells with macrophages as senders. (**B**) The incoming and outgoing interaction strengths. The dot size represents the involved ligand–receptor pairs in each cell type. (**C**) The ligand–receptor pairs predicted via the "CellChat" package with statistical significance (P-value < 0.01). The scale colour represents the level of communication probability from minimum to maximum. (**D**) The network centrality measures of macrophage migration inhibitory factor (MIF) signalling. The depth of colour represents the relative importance of each cell type in MIF signalling.

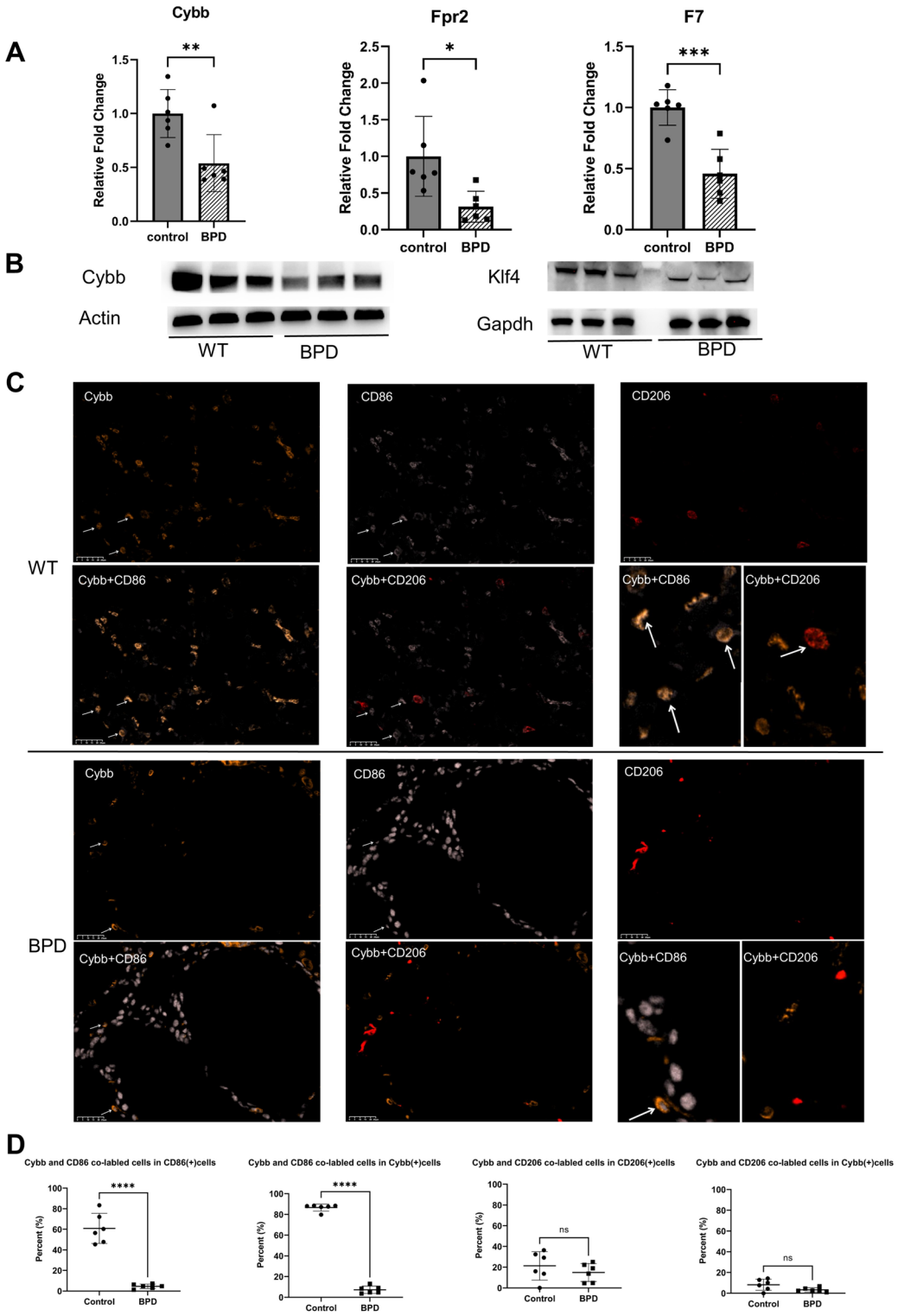

Fig. 7. The validation of hub genes and key pathways in BPD mice models. (**A**) The mRNA expression level of Cybb, Fpr2 and F7 in lungs between hyperoxia and room-air groups evaluated by qRT-PCR. (**B**) The protein level of Cybb and macrophage polarization indicator (Klf4) in lungs between hyperoxia and room-air groups evaluated by WB. (**C**) The representative images of the expression pattern of Cybb(orange) and macrophages markers [M1 phenotype labeled with CD86 (pink) and M2 phenotype labeled with CD206 (red)] in lungs between hyperoxia and room-air groups evaluated by immunofluorescence staining (×80 magnification). Co-labeled cells are indicated with arrows. (**D**) Fluorescence quantification: comparing percentages of co-labeled cells in single-labeled cells and using student t test.

WT, whereas a more irregular and scattered distribution pattern of Cybb independent of CD86 was observed in BPD (Fig. 7C). On average, 60.1% of the CD86(+) cells in WT expressed Cybb, which was significantly greater than the 4.6% in BPD ($P < 0.05$). In addition, 86.5% of the Cybb(+) cells were also CD86(+), compared to 7.3% in BPD ($P < 0.05$). The colocalization of Cybb and CD206 (macrophage M2 marker) also seemed to be greater in WT than BPD; however, the difference did not reach statistical significance ($P > 0.05$) (Fig. 7D). Collectively, the above mentioned results suggested that the downregulation of Cybb in macrophages may be closely related to M1 macrophage infiltration in BPD.

Discussion

BPD is still a considerable threat to preterm infants, and the underlying immune mechanism requires further exploration. Our study demonstrated the reduced expression of Cybb and altered immune characteristics of macrophages in hyperoxia-induced BPD for the first time by exploring cell composition and crosstalk. In the present study, we detected that DEGs between BPD and WT were mostly enriched in immunological processes especially the "leucocyte migration", "PI3K-Akt" and "MAPK" signalling pathways, thus suggesting the vital role of immune cell infiltration in the pathogenesis of BPD. Thus, we predicted the proportions of lung immune cells with CIBERSORT and detected significantly greater proportions of M1 macrophages in BPD than WT. WGCNA was performed to identify genes that were closely related to M1 macrophages, which were subsequently intersected with DEGs to identify macrophage-related DEGs. PPI network analysis identified 15 hub genes among the 172 macrophage-related DEGs. Thevalidations of hub genes at single-cell dataset revealed that Cybb had the closest relationship to macrophages. Cell–cell crosstalk revealed that AT2 cells interacted actively with macrophages through MIF-(CD74 + CD44) signalling. Further experiments validated the role of Cybb in macrophage polarization and important pathways involved BPD development. These findings can help us to better understand the immune characteristics and provide a potential reference for new immunotherapies for BPD.

Inflammation is involved in the pathogenesis of BPD, yet the complex roles of immune cells are not well understood. In view of the important role of macrophages in the lung immune environment, cumulative studies have explored the molecular mechanism of macrophages in BPD. As reported in previous studies, the activation of macrophages in hyperoxia-induced BPD mice not only led to epithelial cells apoptosis and impaired lung parenchyma[27], but also affected fibroblasts and endothelial cells to induce lung matrix remodelling and failed vascularization[27,28]. The transcription factor Klf4 was known to participate in the transcriptional regulation in many diseases including BPD, and Klf4 could induce macrophage polarization by cooperating with Stat6. Klf4 could influence not only the differentiation of monocytes, but also the expression of genes characterizing M1 and M2 macrophages such as iNOS and Arg1[14,29]. Consistent with previous studies, we detected increased infiltration of M1 macrophages and decreased Klf4 expression in BPD mice lung tissues.

Cybb, the key gene revealed by our analysis, encodes gp91phox (NOX2) [a component of the phagocytic nicotinamide adenine dinucleotide phosphate (NADPH) oxidase (NOX) family], which predominantly generates reactive oxygen species (ROS). Cybb is necessary not only for microbial killing and host defense, but also for immune and inflammatory regulation. Studies have explored the important roles of Cybb in lipopolysaccharide (LPS)-induced lung injury, although contradictory results have been reported[30,31], which may be due to different LPS doses. Notably, the expression of Cybb in lung macrophages seemed to play protective roles in the sterile inflammatory response. Germ-free mice with Cybb deficiency developed spontaneous lung inflammation independent of the host microbiota. In addition, alveolar macrophages with Cybb deficiency tended to be proinflammatory with increased cytokine responses and yielded an immune-activated $CD11b^{high}$ subset after germ-free stimulation, such as Toll-like receptor agonists[32]. In a mouse model of zymosan-induced systemic inflammatory response syndrome, Cybb-deficiency in mice was associated with increased chemokine levels, neutrophil infiltration, platelet activation and thrombosis, thus suggesting an anti-inflammatory role for Cybb, especially Cybb derived from alveolar macrophages[33,34]. Moreover, cybb-deficient macrophages not only exhibited increased transcriptional priming of the NOD-like receptor family pyrin domain containing 3 (NLRP3) inflammasome, but also triggered posttranslational NLRP3 activationvia increased K^+ efflux and mitochondrial damage[35]. Consistent with previous findings that Cybb maintained lung homeostasis in sterile inflammation, in this study, we also identified a protective role of Cybb in the pathogenesis of hyperoxia-induced BPD. A specific decrease of Cybb expression in lung macrophages under hyperoxia was detected in our study. Such an abnormal expression pattern of Cybb under hyperoxia may negatively affect lung development and homeostasis. Interestingly, the Cybb gene, which is located on the X chromosome, may offer new insights into the sex-dependent phenotypes of BPD. Overall, the roles of Cybb in inflammation remain controversial based on current evidence. To date, few study have explored Cybb expression in the developing lung under hyperoxia. Our study revealed the potential value of Cybb in protecting neonatal mice from hyperoxia-induced macrophage infiltration and lung inflammation.

The MIF-(CD74 + CD44) signalling pathway was found to be essential for the crosstalk between alveolar epithelial cells and macrophages. MIFis a pleiotropic cytokine, which participates in the upregulation of inflammation by counteracting glucocorticoids and prolonging inflammatory cell survival, angiogenesis signal transduction and endocrine regulation. The cognate receptor of MIF is a complex of the ligand-binding protein CD74 and the signal transducer CD44, which can induce the activation of downstream PI3K-Akt and ERK1/2 signalling pathways[36,37]. It should be noted that the appropriate levels of MIF are essential for lung development, as both the deficiency and overexpression of MIF in mice have been shown to induce alveolar and vascular impairment in newborn mice[38]. One possible explanation for this effect may be the feedback inhibition between MIF and glucocorticoids, which is known to be important for foetal lung maturation. A lack of MIF could induce lower concentrations of circulating glucocorticoids as observed in MIF-knockout mice[39]. In this study, we found that MIF signalling played complex roles in lung development; specifically, MIF signalling mainly occurred between

AT2 cells and endothelial cells in normal controls, whereas MIF signalling mainly involves AT2 cells and macrophages in BPD models under hyperoxia. The alterations in the types of cell–cell crosstalk indicated that both the levels of MIF and the interaction modes of MIF signalling were altered in BPD. We hypothesized that MIF signalling had two sides in lung development: MIF signalling between AT2 cells and endothelial cells might be necessary for alveolarization and angiogenesis, whereas the involvement of macrophages in MIF signalling after hyperoxia might promote inflammation and hinder lung immaturity.

There were several limitations of our study. Although previous studies and preliminary experimental results have indicated that our analyses were reliable, to better understand the function of macrophage-derived Cybb in BPD, further research is needed to determine the complex roles of Cybb in inflammation in different contexts. Moreover, the roles of Cybb in macrophage polarization may be lung tissue-specific, thus the application of Cybb as a diagnostic marker in clinics might be limited.

Conclusion

In summary, our data indicated that macrophage activation (towards M1 polarization) after hyperoxia played important roles in promoting BPD-like lung injury, which was possibly correlated with the reduced expression of Cybb in macrophages. Besides, the involvement of macrophages in MIF signalling might also play important roles in BPD pathogenesis. The development of therapeutic strategies targeting these potential factors might reverse hyperoxia-induced noninfectious inflammation of developing lungs. The activation of Cybb might serve as a potential therapeutic target by restoring the balance of lung macrophages in hyperoxia-induced BPD.

Data availability

The data of the current study are available from the corresponding author on reasonable request.

Received: 23 February 2024; Accepted: 22 August 2024
Published online: 29 August 2024

References

1. Jobe, A. H. & Bancalari, E. Bronchopulmonary dysplasia. *Am. J. Respir. Crit. Care Med.* **163**(7), 1723–1729 (2001).
2. Northway, W. H. Jr., Rosan, R. C. & Porter, D. Y. Pulmonary disease following respirator therapy of hyaline-membrane disease. Bronchopulmonary dysplasia. *N. Engl. J. Med.* **276**(7), 357–368 (1967).
3. Harris, C. & Greenough, A. The prevention and management strategies for neonatal chronic lung disease. *Expert Rev. Respir. Med.* **17**(2), 143–154 (2023).
4. Karatza, A. A., Gkentzi, D. & Varvarigou, A. Nutrition of infants with bronchopulmonary dysplasia before and after discharge from the neonatal intensive care unit. *Nutrients.* **14**(16), 3311 (2022).
5. DeMauro, S. B. Neurodevelopmental outcomes of infants with bronchopulmonary dysplasia. *Pediatr. Pulmonol.* **56**(11), 3509–3517 (2021).
6. Harris, C., Morris, S., Lunt, A., Peacock, J. & Greenough, A. Influence of bronchopulmonary dysplasia on lung function in adolescents who were born extremely prematurely. *Pediatr. Pulmonol.* **57**(12), 3151–3157 (2022).
7. Harris, C., Lunt, A., Bisquera, A., Peacock, J. & Greenough, A. Lung function and exercise capacity in prematurely born young people. *Pediatr. Pulmonol.* **55**(9), 2289–2295 (2020).
8. Ambalavanan, N. *et al.* Cytokines associated with bronchopulmonary dysplasia or death in extremely low birth weight infants. *Pediatrics.* **123**(4), 1132–1141 (2009).
9. Stenson, B. J. *et al.* Oxygen saturation and outcomes in preterm infants. *N. Engl. J. Med.* **368**(22), 2094–2104 (2013).
10. Ozdemir, R. *et al.* Clarithromycin in preventing bronchopulmonary dysplasia in *Ureaplasma urealyticum*-positive preterm infants. *Pediatrics.* **128**(6), e1496-1501 (2011).
11. Papagianis, P. C., Pillow, J. J. & Moss, T. J. Bronchopulmonary dysplasia: Pathophysiology and potential anti-inflammatory therapies. *Paediatr. Respir. Rev.* **30**, 34–41 (2019).
12. Johnson, B. H. *et al.* A critical role for the IL-1 receptor in lung injury induced in neonatal rats by 60% O2. *Pediatr. Res.* **66**(3), 260–265 (2009).
13. Nold, M. F. *et al.* Interleukin-1 receptor antagonist prevents murine bronchopulmonary dysplasia induced by perinatal inflammation and hyperoxia. *Proc. Natl. Acad. Sci. U. S. A.* **110**(35), 14384–14389 (2013).
14. Hirani, D. *et al.* Macrophage-derived IL-6 trans-signalling as a novel target in the pathogenesis of bronchopulmonary dysplasia. *Eur. Respir. J.* **59**(2), 2002248 (2022).
15. Hirani, D. V. *et al.* CXCL10 deficiency limits macrophage infiltration, preserves lung matrix, and enables lung growth in bronchopulmonary dysplasia. *Inflamm. Regener.* **43**(1), 52 (2023).
16. Dong, J. *et al.* MicroRNA-mRNA interactions in a murine model of hyperoxia-induced bronchopulmonary dysplasia. *BMC Genom.* **13**, 204 (2012).
17. Xia, S. *et al.* Neonatal hyperoxia induces activated pulmonary cellular states and sex-dependent transcriptomic changes in a model of experimental bronchopulmonary dysplasia. *Am. J. Physiol. Lung Cell. Mol. Physiol.* **324**(2), L123-l140 (2023).
18. Steenwyk, J. L. & Rokas, A. ggpubFigures: Colorblind-friendly color palettes and ggplot2 graphic system extensions for publication-quality scientific figures. *Microbiol. Resour. Announc.* **10**(44), e0087121 (2021).
19. Wu, T. *et al.* clusterProfiler 4.0: A universal enrichment tool for interpreting omics data. *Innovation (Cambridge (Mass)).* **2**(3), 100141 (2021).
20. Newman, A. M. *et al.* Robust enumeration of cell subsets from tissue expression profiles. *Nat. Methods.* **12**(5), 453–457 (2015).
21. Langfelder, P. & Horvath, S. WGCNA: An R package for weighted correlation network analysis. *BMC Bioinform.* **9**, 559 (2008).
22. Szklarczyk, D. *et al.* The STRING database in 2023: Protein–protein association networks and functional enrichment analyses for any sequenced genome of interest. *Nucleic Acids Res.* **51**(D1), D638-d646 (2023).
23. Chin, C. H. *et al.* cytoHubba: Identifying hub objects and sub-networks from complex interactome. *BMC Syst. Biol.* **8**(Suppl 4), S11 (2014).
24. Butler, A., Hoffman, P., Smibert, P., Papalexi, E. & Satija, R. Integrating single-cell transcriptomic data across different conditions, technologies, and species. *Nat. Biotechnol.* **36**(5), 411–420 (2018).
25. Jin, S. *et al.* Inference and analysis of cell–cell communication using Cell Chat. *Nat. Commun.* **12**(1), 1088 (2021).
26. Bermudez, S., Khayrullina, G., Zhao, Y. & Byrnes, K. R. NADPH oxidase isoform expression is temporally regulated and may contribute to microglial/macrophage polarization after spinal cord injury. *Mol. Cell. Neurosci.* **77**, 53–64 (2016).
27. Thébaud, B. *et al.* Bronchopulmonary dysplasia. *Nat. Rev. Dis. Primers.* **5**(1), 78 (2019).

28. Riccetti, M. R., Ushakumary, M. G., Waltamath, M., et al. Maladaptive functional changes in alveolar fibroblasts due to perinatal hyperoxia impair epithelial differentiation. *JCI Insight.* **7**(5) (2022).
29. Liao, X. *et al.* Krüppel-like factor 4 regulates macrophage polarization. *J. Clin. Investig.* **121**(7), 2736–2749 (2011).
30. Menden, H. L. *et al.* Nicotinamide adenine dinucleotide phosphate oxidase 2 regulates LPS-induced inflammation and alveolar remodeling in the developing lung. *Am. J. Respir. Cell Mol. Biol.* **55**(6), 767–778 (2016).
31. Zhang, W. J., Wei, H. & Frei, B. Genetic deficiency of NADPH oxidase does not diminish, but rather enhances, LPS-induced acute inflammatory responses in vivo. *Free Radic. Biol. Med.* **46**(6), 791–798 (2009).
32. Bhattacharya, S. *et al.* Macrophage NOX2 NADPH oxidase maintains alveolar homeostasis in mice. *Blood.* **139**(19), 2855–2870 (2022).
33. Hook, J. S. *et al.* Nox2 regulates platelet activation and NET formation in the lung. *Front. Immunol.* **10**, 1472 (2019).
34. Potera, R. M. *et al.* Alveolar macrophage chemokine secretion mediates neutrophilic lung injury in Nox2-deficient mice. *Inflammation.* **42**(1), 185–198 (2019).
35. Monjarret, B., Shour, S., Benyoucef, A., et al. NOX2 deficiency enhances priming and activation of the NLRP3 inflammasome. *J. Allergy Clin. Immunol.* (2023).
36. Jankauskas, S. S., Wong, D. W. L., Bucala, R., Djudjaj, S. & Boor, P. Evolving complexity of MIF signaling. *Cell. Signal.* **57**, 76–88 (2019).
37. Kang, I. & Bucala, R. The immunobiology of MIF: Function, genetics and prospects for precision medicine. *Nat. Rev. Rheumatol.* **15**(7), 427–437 (2019).
38. Sun, H. *et al.* Small molecular modulation of macrophage migration inhibitory factor in the hyperoxia-induced mouse model of bronchopulmonary dysplasia. *Respir. Res.* **14**(1), 27 (2013).
39. Kevill, K. A. *et al.* A role for macrophage migration inhibitory factor in the neonatal respiratory distress syndrome. *J. Immunol. (Baltimore, Md.: 1950)* **180**(1), 601–608 (2008).

Author contributions

F.L. designed the entire study. Y.H. and D.L. performed the experiment. Y.H. and M.Z. performed the data analysis. Y.H. wrote the article. Y.H., D.L., M.Z. and F.L. revised the manuscript. All authors approved the final manuscript. All authors contributed to the article and approved the submitted version.

Funding

This study was funded by grants from the National Key Research and Development Program of China (2022YFC2704801) and the Natural Science Foundation of Chongqing (cstc2021jcyj-msxmX0257). Science and health key project of Chongqing Health Commission (2023ZDXM024). Chongqing Research Center for Prevention & Control of Maternal and Child Diseases and Public Health.

Competing interests

The authors declare no competing interests.

Additional information

Supplementary Information The online version contains supplementary material available at https://doi.org/10.1038/s41598-024-70877-7.

Correspondence and requests for materials should be addressed to F.L.

Reprints and permissions information is available at www.nature.com/reprints.

Publisher's note Springer Nature remains neutral with regard to jurisdictional claims in published maps and institutional affiliations.

Open Access This article is licensed under a Creative Commons Attribution-NonCommercial-NoDerivatives 4.0 International License, which permits any non-commercial use, sharing, distribution and reproduction in any medium or format, as long as you give appropriate credit to the original author(s) and the source, provide a link to the Creative Commons licence, and indicate if you modified the licensed material. You do not have permission under this licence to share adapted material derived from this article or parts of it. The images or other third party material in this article are included in the article's Creative Commons licence, unless indicated otherwise in a credit line to the material. If material is not included in the article's Creative Commons licence and your intended use is not permitted by statutory regulation or exceeds the permitted use, you will need to obtain permission directly from the copyright holder. To view a copy of this licence, visit http://creativecommons.org/licenses/by-nc-nd/4.0/.

© The Author(s) 2024